

# Modelling Approach for Vented Lean Deflagrations in Non-Rigid Enclosures

Vendra C.M.R.<sup>1</sup>, Wen J.<sup>1,\*</sup>

<sup>1</sup> *Warwick Fire, School of Engineering, University of Warwick, Coventry, UK*

*\*Corresponding author's email: [jennifer.wen@warwick.ac.uk](mailto:jennifer.wen@warwick.ac.uk)*

## ABSTRACT

Containers are being considered for hydrogen fuel installations either be at the refuelling station housing the compressor and pumps or for portable standalone power generation units housing the fuel cell and its accessories. Identifying the hazards associated with these kind of container applications is essential for its design, safe operations and in mitigating any accidental risks. Recently both numerical study and experiment have been performed to ascertain the level of hazards and its possible mitigation methods. This paper presents the numerical modelling and the simulations performed using the HYFOAM solver, developed in-house using the opensource CFD toolkit OpenFOAM libraries. The turbulent flame deflagration is modelled using the flame wrinkling combustion model. Additional sub-models are added to the combustion model to account for the dominant flame instabilities present in the vented lean hydrogen-air mixtures deflagrations. The 20-foot ISO containers of dimensions 20' x 8' x 8'.6" filled with homogenous mixture of hydrogen-air at different concentration, with and without model obstacles are considered for numerical simulations. The numerical predictions are first validated against the experiments carried out by Gexcon as part of the HySEA project supported by the Fuel Cells and Hydrogen 2 Joint Undertaking (FCH 2 JU) under the Horizon 2020 Framework Programme for Research and Innovation. The container wall deflections were found to be considerable in the experiments, contributing to the overpressure through acoustic and structural resonance responses. The preliminary CFD predictions also indicated that the container wall deflections are having considerable effect on the generated numerical overpressures trends, especially the peak negative pressure generated within the container is overestimated. Hence to account for the container wall deflections, the Fluid Structure Interactions (FSI) are also included in the numerical modelling. The CFD and FSI are coupled in pseudo two-way approach. The final numerical predictions are presented with and without the FSI.

**KEYWORDS:** Hydrogen, vented deflagrations, ISO containers, OpenFOAM, fluid structure interaction.

## INTRODUCTION

Hydrogen as an energy carrier can play a very important role in reducing the global greenhouse gas emissions. As such hydrogen fuel usage is steadily on rise for both stationary and mobile energy applications. The 20-foot or 40-foot shipping containers are being considered for housing portable hydrogen fuel cell power units and other accessories, even in case of the hydrogen refuelling station, the compressor, pumps and other auxiliary units are housed in these container units. The shipping containers are easy to handle and provide adequate protection to the process equipment. Hydrogen gas has unique physical properties especially the wide flammability limits, very lean mixtures can ignite and lead to explosion. Shipping containers are well designed for handling the cargos but not for any other applications, hence process safety, hazards identification and consequence analysis is essential to safeguard these hydrogen installations.

Explosion venting is a preventive measure used to reduce the overpressures within an enclosure and confinements, during any accidental explosion. Experiments have been performed in last few

Proceedings of the Ninth International Seminar on Fire and Explosion Hazards (ISFEH9), pp. 393-402

Edited by Snegirev A., Liu N.A., Tamanini F., Bradley D., Molkov V., and Chaumeix N.

Published by St. Petersburg Polytechnic University Press

ISBN: 978-5-7422-6496-5 DOI: 10.18720/spbpu/2/k19-81

decades to understand the factor affecting the vented explosion process [1-8]. It was found experimentally, flame instabilities have a dominating effect on vented deflagrations process apart from the flame-turbulence interactions [1, 5-6]. Both thermodynamic and hydrodynamic instabilities influence the process at different stages of the flame evolution. Hydrodynamic and thermodynamic diffusive Darrieus-Landau instabilities are dominant at the early stages of the flame propagations, leading to cellular and wrinkled flame front. The venting of hot gases through the vent opening setup Helmholtz oscillations due to inertial effects of the expelled gases. The nozzle effect at vent, results in flame and hot combustion product accelerations into relatively cold outside ambient conditions, give rise to Rayleigh-Taylor instabilities at the flame interface. These instabilities are modelled numerically as mutually exclusive events using either an algebraic expression or solving a transport equation [5-6]. Lewis number ( $Le$ ) effects also plays an important role in flame propagation in lean hydrogen-air mixtures [9-10]. Its influence is evident from the fact that ' $Le$ ' factor is added to the most of lean hydrogen turbulent flame speed correlations.

Experiments for homogenous mixtures in full scale 20 foot ISO container have been carried out by Gexcon [12] as part of the HySEA project supported by the Fuel Cells and Hydrogen 2 Joint Undertaking (FCH 2 JU) under the Horizon 2020 Framework Programme for Research and Innovation. It was observed in the experiments that the container corrugated wall was not rigid enough and structural deformation/vibrations altered the overpressure trends. The Fluid Structure Interactions (FSI) is required for numerical modelling of container wall deflections. One of such study was done by [14], wherein the response of an offshore fire partition wall is studied against dynamic explosion overpressure loads. A spatial mapping of deflagration overpressure transients obtained with Computational Fluid Dynamics (CFD) code FLACS is used in combination with a Non-Linear Finite Element analysis IMPETUS Afea solver. The study of the steel structures in natural fires was attempted by employing the CFD and FE in one-way coupled numerical methods by [15]. In their work coupling is done between CFD and FE by dedicated scripts and computed the heat transfer between gas and solid phases. The emphasis was on the proper calculation of temperature field inside the structural members. In the present study, numerical modelling and simulations are being conducted to further aid our understanding of the vented hydrogen gas deflagrations in ISO container units using the opensource Computational Fluid Dynamics (CFD) code OpenFOAM [16] solver HyFOAM. The following sections describe the HyFOAM solver and the predicted numerical results.

## NUMERICAL MODELLING

HyFOAM solver is developed for vented lean hydrogen applications using the open source toolkit libraries of OpenFOAM [16]. The governing Navier-Stokes equations are solved in explicit Large Eddy Simulation (LES) context for collocated finite volume mesh. The closure for the subgrid viscosity is computed through a transport equation for subgrid kinetic energy [17]. The pressure velocity coupling is solved in Pressure-Implicit Split Operator (PISO) method. The advective terms are discretized in second-order accurate limited-linear scheme and the temporal term are discretized using a fully implicit, second-order accurate three-time-level method [16]. Hence the combination of these schemes renders the developed HyFOAM solver second-order accurate in both spatial and temporal coordinates. The complete set of governing equations are solved sequentially with iteration over the explicit coupling terms to obtain convergence.

### Combustion model

The Flame Surface Wrinkling Model developed by [18] is used for simulating the turbulent deflagrations. The Flame Surface Wrinkling Model is based on flamelet concept treating the flame as a thin interface between burnt and unburnt gases. This interface is corrugated and wrinkled due to contribution factor and the flow turbulence. The unburnt zone volume fraction is denoted as a

regress variable ( $b$ ), taking representative values of  $b = 1$  in fresh gases and  $b = 0$  in fully burnt gas. The transport equation for the resolved part of regress variable ( $b$ ) is given as [18, 19]

$$\frac{\partial \bar{\rho} \tilde{b}}{\partial t} + \nabla \cdot (\bar{\rho} \tilde{U} \tilde{b}) - \nabla \cdot (\bar{\rho} \mu_{sgs} \nabla \tilde{b}) = -\bar{\rho}_u S_L \Xi |\nabla \tilde{b}|, \quad (1)$$

where  $\Xi$  is subgrid flame wrinkling, can be regarded as the turbulent to laminar flame speed ratio and is formally related to the flame surface density by  $\Sigma = \Xi |\nabla \tilde{b}|$ . Symbols ( $\bar{\quad}$ ) and ( $\tilde{\quad}$ ) represents the filtered and the density weighted filtering operations respectively.  $\rho$  is the density,  $S_L$  is laminar flame speed and  $\mu_{sgs}$  is the subgrid turbulent diffusion coefficient. The subscripts indicates conditioning on the unburned gases region. The resolved filtered unburned gas volume fraction  $\bar{b}$  is related to Favre filtered  $\tilde{b}$  through  $\bar{\rho}_u \bar{b} = \bar{\rho} \tilde{b}$ . The closure for the sub-grid wrinkling ( $\Xi$ ) can be provided either by a balanced transport equation or by an algebraic expression assuming equilibrium between the source terms, whereas the transport model allows for non-equilibrium effects between the source terms. The transport equation model closure for the  $\Xi$  is

$$\frac{\partial \bar{\rho} \Xi}{\partial t} + \hat{U}_s \nabla \Xi = \bar{\rho} G \Xi - \bar{\rho} R (\Xi - 1) + \bar{\rho} \max(\sigma_s - \sigma_t, 0) \Xi, \quad (2)$$

where  $\tilde{U}_s$  is the surface filtered local instantaneous velocity of the flame, modelled as

$$\tilde{U}_s = \tilde{U} + \left( \frac{\bar{\rho}_u}{\bar{\rho}} - 1 \right) S_L \Xi n_f - \frac{\nabla \cdot (\bar{\rho} \mu_{sgs} \nabla \tilde{b})}{\bar{\rho} |\nabla \tilde{b}|} n_f. \quad (3)$$

The flame normal is  $n_f = \nabla \tilde{b} / |\nabla \tilde{b}|$ ,  $\sigma_s$  and  $\sigma_t$  are the surface filtered resolved strain-rates relating to the surface filtered local instantaneous velocity of the flame ( $\tilde{U}_s$ ) and surface filtered effective flame velocity of the flame surface ( $\tilde{U}_t$ ), modelled as

$$\begin{aligned} \sigma_t &= \nabla \cdot (\tilde{U} + S_L \Xi n_f) - n_f \cdot \left( \nabla (\tilde{U} + S_L \Xi n_f) \right) \cdot n_f, \\ \sigma_s &= \frac{\nabla \cdot \tilde{U} - n_f \cdot (\nabla \tilde{U}) \cdot n_f}{\Xi} + \frac{(\Xi + 1) \left( \nabla (S_L n_f) - n_f \cdot \left( \nabla (S_L n_f) \right) \cdot n_f \right)}{2\Xi}. \end{aligned} \quad (4)$$

The terms  $G\Xi$  and  $R(\Xi - 1)$  in Eq. (2) represent the sub-grid turbulence generation and removal rates, with  $G$  and  $R$  as rate coefficients requiring modelling. The modelling of these terms is based on flame-speed correlation of [19] are shown below

$$\begin{aligned} G &= R \frac{\Xi_{eq} - 1}{\Xi_{eq}} \quad \text{and} \quad R = \frac{0.28}{\tau_\eta} \frac{\Xi_{eq}^*}{\Xi_{eq}^* - 1}, \\ \Xi_{eq} &= 1 + 2(1-b) (\Xi_{eq}^* - 1) \quad \text{and} \quad \Xi_{eq}^* = 1 + \frac{0.46}{Le} \text{Re}_t^{0.25} \left( \frac{\hat{u}}{S_{Lo}} \right)^{0.3}, \end{aligned} \quad (5)$$

where  $\tau_\eta$  is the Kolmogorov time scale,  $\hat{u}$  is the sub grid turbulence intensity,  $\text{Re}_t$  is the turbulent Reynolds number,  $\Xi_{eq}$  is the equilibrium wrinkling, and  $\Xi_{eq}^*$  is turbulent flame speed correlation.

The modelling of the terms  $\Xi_{eq}^*$  in Eq. (5) is improved in present work for lean turbulent premixed combustion by including the Lewis number ( $Le$ ) factor in the turbulent flame speed correlation. The algebraic reaction rate closure, MFSD proposed in [20] is adopted in the present study. This model has been successfully applied to both pure and mixed fuels, under varying Lewis number conditions [21] [22], in both RANS and LES contexts. Figure 1 shows the MFSD model predictions for the turbulent flame speed ( $S_T$ ) for lean equivalence ratio between 0.4 and 0.8 along with Goulier's expression [23] is compared with the experimental measured values of [24].

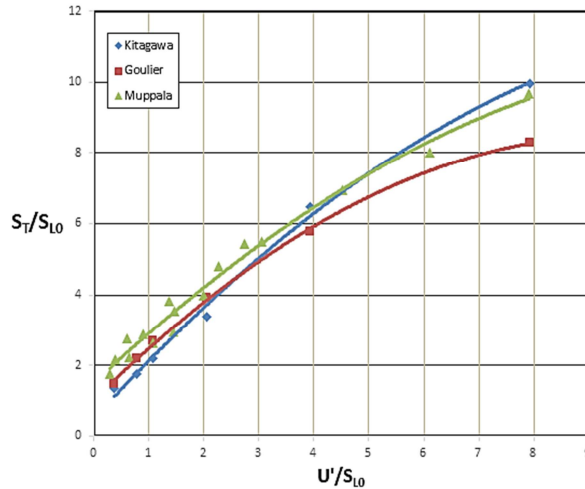


**Fig. 1.** Comparison of turbulent flame speed correlation of [20] [23] with the experimental results of [24].

The Darrieus–Landau and thermodiffusive instabilities affect the flame propagations in lean mixtures leading to formation of cusps and turfs, cellular structures at the flame front. These instabilities are modelled considering the simple analytical expression proposed by [7] as

$$\Xi_{DL} = \max\left(1, \alpha_1 (\Delta/\lambda_c)^{1/3}\right), \quad (6)$$

where,  $\lambda_c$  is the cutoff wavelength of unstable scales and  $\alpha_1$  is the coefficient to account for uncertainty in  $\lambda_c$ ,  $\Delta$  is the LES filter size. The values of  $\lambda_c = 7$  mm and  $\alpha_1 = 1.35$  are used in the current simulations to match the initial flame propagations [7]. The Rayleigh-Taylor instability is modelled as transport equation similar in lines to Eq. (2) purposed in [7] is shown below

$$\frac{\partial \bar{\rho} \Xi_{RT}}{\partial t} + \hat{U}_S \nabla \Xi_{RT} = \bar{\rho} G_{RT} (\Xi_{RT} - 1) - \bar{\rho} R_{RT} (\Xi_{RT} - 1), \quad (7)$$

where,  $G_{RT} (\Xi_{RT} - 1)$  and  $R_{RT} (\Xi_{RT} - 1)$  are rate of generation and removal of sub-grid wrinkling due to RT-instability. These coefficients are modelled as

$$G_{RT} = 2 \left( k_{RT} \frac{\sigma - 1}{\sigma + 1} \bar{a} \bar{n}_f \right)^{1/2} \quad \text{and} \quad R_{RT} = \frac{8\sigma S_L k_{RT}}{\pi}, \quad (8)$$

where  $\bar{a}$  is the flame acceleration evaluated from the flame displacement velocity,  $\sigma$  is the flame expansion ratio,  $k_{RT}$  is the unstable wavenumber associated with the RT-instability assumed to be constant for a given fuel, a value of  $6 \text{ m}^{-1}$  is used in the present study. The unstrained laminar flame

speed ( $S_L$ ) function of equivalence ratio ( $\phi = 1/\lambda$ ) for lean hydrogen-air mixture is adopted from the numerical study carried out by [25], expressed as power law expression as

$$S_L = S_{L0} (\lambda, P)^{\alpha(\lambda, P)}, \quad (9)$$

$$S_{L0} = 499.63 - 308.60\lambda + 48.887\lambda^2 - 76.238P + 4.825P^2 + 45.813\lambda P - 2.926\lambda P^2 - 7.163\lambda^2 P + 0.436\lambda^2 P^2,$$

$$\alpha(\lambda, P) = 1.85175 - 0.70875\lambda + 0.50171\lambda^2 - 0.19366P + 0.0067834P^2 + 0.27495\lambda P - 0.0088924\lambda P^2 - 0.052058\lambda^2 P + 0.00146015\lambda^2 P^2,$$

where  $S_L$  is in cm/s,  $P$  is the pressure (bar), and  $T_u$  is the unburnt gas temperature (K). The above correlation is valid between the equivalence ratios ( $\phi$ ) of 0.33 and 0.47, pressures range of 1 bar  $\leq P \leq 8.5$  bar, and temperature range of 300 K  $\leq T \leq 800$  K with reference temperature state  $T_{u0} = 300$  K. The flame wrinkling factor in Eq. (1) is updated with sub-models for flame instabilities as

$$\Xi = \Xi_t * \Xi_{DL} * \Xi_{RT}. \quad (10)$$

Equations (1)-(10) constitute the combustion model for lean hydrogen mixture deflagration in the HyFOAM solver.

## EXPERIMENT DETAILS

The typical 20-ft ISO container of dimensions 20'x 8'x 8'.6" used in the experiments at Gexcon is shown in Fig. 2. The walls of the container are corrugated and 2 mm in thickness. The dimensions of the container inside are 5.867 m x 2.385 m x 2.352 m. The container doors are having dimensions of 2.225 m high, 1.114 m wide and 50 mm thick, were kept open in perpendicular position to the container (Fig. 5 a) during the door open venting experiments.



**Fig. 2.** Standard 20 ft. ISO container used in the experiments [12].

The instrumentation and obstacle are held in a steel frame fixed to the floor of the container. The frame is constructed using U-beams (200 mm x 75 mm) steel sections, shown in Fig. 3 a. A bottle basket of 20 gas bottles held in a basket representative of a dense congestion is used inside the container as model obstacle. The individual gas bottles are 50-litre steel cylinders of diameter 0.23 m and height 1.66 m from the floor to the top of the valve. The cylinders are mounted in a square basket made from 50 mm x 50 mm square steel pipes and the gaps between the bottles spacers fix fixed by spacers to 5 mm. The overall external dimensions of the bottle basket are about 1.27 m x 1.04 m as shown in Fig. 3 b. The pressure sensors are placed symmetrically in the steel frame at distance of 0.86 m for P1 & P2, 2.45 m for P3 & P4, 4.0 m P5 & P6 and 5.56 m for P7 & P8 from

the backend container wall and 0.2 m elevation from the container floor. The pressure probes placed outside the open doors of the container are at an elevation of 1.65 m and at 5 m (P9), 10 m (P10) and 15 m (P11) distance from the open-end along the centreline, as shown in Fig. 4.

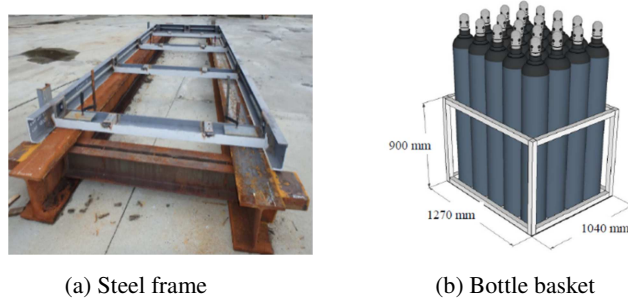


**Fig. 3.** Congestion and model obstacles with in the containers [12].

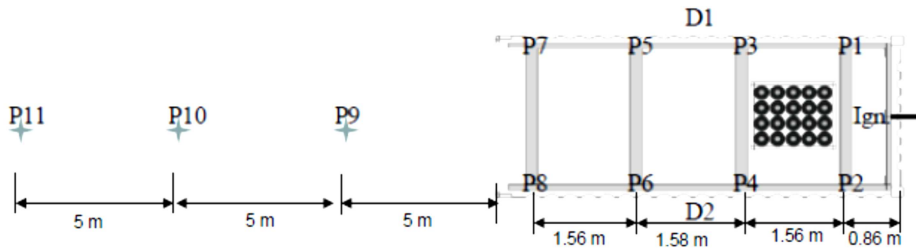


**Fig. 4.** Overpressure monitoring points with respect to the frame and container [12].

The outside container pressure sensor are fitted on to a plate fixed at the top of the vertical tube, about 1.65 m above the ground, measuring the side-on pressure. D1 and D2 are two laser probes pointing the mid-section of either container side wall to measure the container wall deflections with respect to time from start of ignition. An electric inductive spark located at the back wall of the container, along the centreline, and at mid height is used to ignite the homogenous mixtures.

## NUMERICAL SETUP

The numerical computational domain with and without obstacles inside the container are shown in Fig. 5. The ignition of the homogenous hydrogen-air mixture is initiated by a spherical hot patch of diameter 2 cm at the centre of the back end wall at the mid height of the container with products composition and temperature, mimicking the electric spark used in the experiments. The patch diameter was chosen such that it contains minimum 10-12 cells to establish the initial flame propagation.

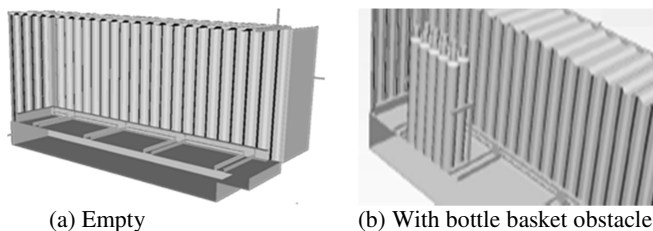


**Fig. 5.** The standard 20-ft ISO container with model obstacles.

The container walls are assumed to be rigid initially but later modelled as moving wall to accommodate the fluid structure interactions (FSI). The boundary conditions applied to the container walls were non-slip and adiabatic for the chamber walls and ground. The ‘totalPressure’ and ‘pressureInletOutletVelocity’ boundary conditions combination were used for pressure and velocity respectively at the open boundaries. This combination of pressure and velocity boundary condition allows for the flow reversal at the open boundary. To validate the numerical modelling approach in the present study, three experimental scenarios (case studies) are considered: I) Case-1: Configuration of no obstacles, steel frame and doors fully open with 15 % vol. hydrogen concentration as shown in Fig.5 a; II) Case-2: Configuration with bottle basket close to the back end, steel frame and doors fully open with 15 % Vol. hydrogen concentration, shown in Fig. 5 b. The ‘SnappyHexMesh’ utility in OpenFOAM [16] is been used to generate the finite volume. A non-uniform cell size of 3 mm was used in the ignition region, and 5-15 mm cell size inside the chamber and in the area immediately outside the chamber to resolve the external deflagration. The total finite volume cells in computational mesh are approximately between 8~12 million for the simulations considered in the present study.

## FLUID STRUCTURE INTERACTIONS

The experiments conducted in HySEA Phase-1 homogenous mixtures at Gexcon are 12 in number with containers doors open, back wall ignition, involving change in concentration and model obstacles. The complete details about the HySEA Phase-1 experimental campaign can be found in the [12]. Tests 1 and 2, which are repeated experiments at 15% H<sub>2</sub> concentration in empty container, are considered to infer the structural response of the container. Figure 6 shows plots of the experimental overpressure and container side wall deflection for frame only tests.

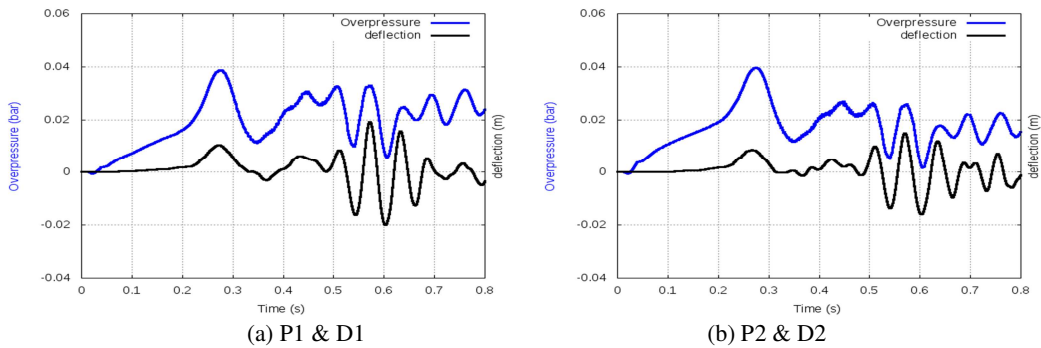


**Fig. 6.** Test 1: 15% H<sub>2</sub>, empty, overpressure and deflection trace curves.

The overpressure at P1 and P2 probes and the container side wall deflections D1 and D2 respectively are almost in quasi-equilibrium. The peak overpressures are recorded at P1 and P2 location for the back wall ignition. A fully coupled fluid structure interactions in CFD, will have two-way interaction i.e. the influence of the fluid forces on the solid structures and the displacements of the solid boundary on the fluid flows. In the present study, a pseudo two-way interactions approach is being used to improve the CFD predictions, wherein the structural displacements against the overpressures from the experiments are fit into single degree of freedom (SDOF) of motion for a spring-mass-damper system, shown in Fig. 7.

The equation of motion for SDOF system shown in Eq. (11), is solved for  $x(t)$  and used in CFD simulations. The structural displacements  $x(t)$  are applied to the container wall through a moving wall boundary condition. Thus both the overpressures and wall deflections are computed during the runtime of the CFD simulations

$$F(t) = Kx(t) + M \frac{d^2x(t)}{dt^2} + B \frac{dx(t)}{dt}, \tag{11}$$

where,  $M$  is the mass of the system (neglecting the spring mass),  $B$  is the damping coefficient (N·s/m),  $K$  is the spring stiffness factor (N/m),  $F(t)$  is the driving force, and  $x(t)$  is the response of the system to the driving force (displacements).

### RESULTS AND DISCUSSIONS

In the context of the container FSI,  $F(t)$  represents the mean deflagration overpressure observed at the P1 probe location and  $x(t)$  corresponds to the container wall deflections measured by the D1 laser probe. The constants ‘ $m$ ’, ‘ $c$ ’ and ‘ $k$ ’ in Eq. (11) are estimated to be  $6.09 \times 10^{-5} \text{ kg/m}^2$ ,  $0.009 \text{ N·s/m}^3$  and  $3.84 \text{ Pa/m}$  respectively, such that the scaled driving force (i.e. product of  $F(t)$  and flexibility factor,  $1/K$ ) is in good match with the predicted displacement  $x(t)$ , also  $b$  is adjusted to match the pressure oscillations frequency. Figure 8 shows the experimental and modelled deflections for case 1.

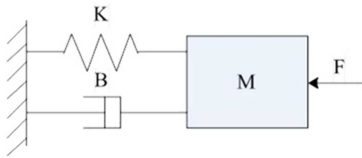


Fig. 7. Single degree of freedom motion system.

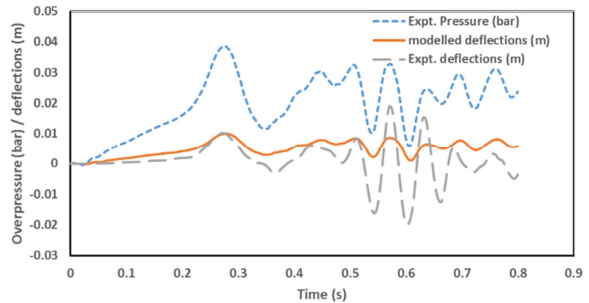


Fig. 8. Pressure trace curve for P1 pressure probe location along.

The wall central deflection  $x(t)$  is obtained from solving the Eq. (11) at the wall boundary, the displacements on each wall surface is applied in the form of an ellipsoidal contours, similar to the results obtained in [26] using the software’s FLACS and IMPETUS for CFD and FE calculations respectively. The CFD prediction with and without FSI along with the experimental results for empty and with bottle basket obstacles in container are shown in Fig. 9.

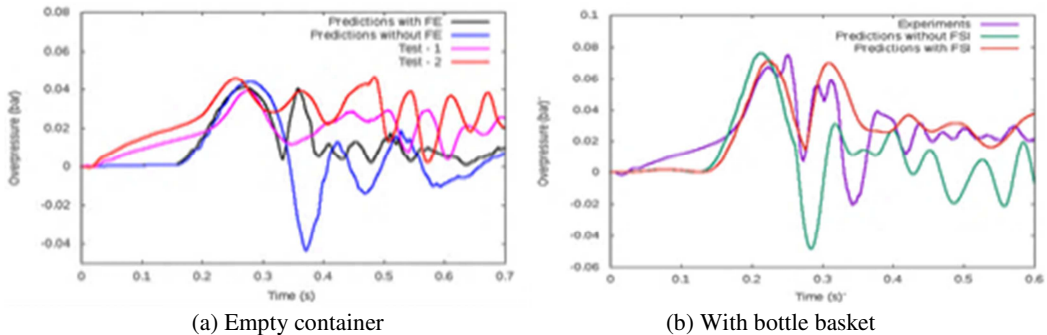


Fig. 9. Pressure trace curve for P1 pressure probe location along with experiment measurements.

The peak pressure is obtained at P1 (P2) location for back wall ignition. The hot gas continued to expand through the open doors without any flow constriction at the vent section, this leads to decreasing overpressure trend along the length of the container. The pressure trace curves in the container are oscillatory in later part due to the contributions from the Helmholtz oscillation generated by venting of the bulk of the hot gases. In case of obstacles, there is a second overpressure peak with slightly less in magnitude to that of the first overpressure peak. The second overpressure peak is due to the flame accelerations through and around the obstacles. The distinct feature present in the ‘without FSI’ numerical prediction Fig. 9, is the large magnitude for the first negative pressure generated after the peak overpressure, which is almost absent in the experimental results is improved in ‘with FSI’ numerical predictions. Therefore, the coupled CFD and FSI approach has improved the overall CFD overpressure prediction trends.

## CONCLUSIONS

The 20-ft ISO containers are being considered for hydrogen installations either for developing self-contained portable power generation units using the fuel cell technologies or for housing compressor/pumps at hydrogen refueling stations. The possible scenarios of lean hydrogen-air deflagrations in these containers are being studied numerically in the present study. Experimental data from full scale 20-foot container tests carried out by Gexcon, are used for numerical modelling validations. The modification to flame wrinkling factor and turbulent flame speed considered in the present. To further improve the overpressure trends, the CFD simulations are coupled with FSI in a pseudo two-way interactions, where in the spring-mass-damper motion equation once evaluated for experimental structural responses, are then solved dynamically at the wall boundary to obtain the displacements based on the mean peak overpressure at P1 probe located inside the container. The final numerical results of the coupled CFD and FSI are very promising in predicting the experimental trends within the experimental uncertainties. The major improvement is in correction of the peak negative pressures observed after the peak overpressure in the results. Shown in Fig. 9, the vented deflagration for 15% vol. concentration of hydrogen in the container with model obstacles produced nearly twice the overpressures in magnitude to that of the empty container. Such information is very vital in designing of the vents for the process equipment and also defining the safety distances around the hydrogen process installations.

## ACKNOWLEDGEMENTS

The HySEA project ([www.hysea.eu](http://www.hysea.eu)) receives funding from the Fuel Cells and Hydrogen Joint Undertaking under grant agreement No 671461. This Joint Undertaking receives support from the European Union’s Horizon 2020 research and innovation programme and United Kingdom, Italy, Belgium and Norway.

## REFERENCES

- [1] P.J. Mccann, G.O. Thomas, D.H. Edwards, Geodynamics of Vented explosions Part I: Experimental studies, *Combust. Flame* 59 (1985) 233-250.
- [2] M.G. Cooper, M. Fairweather, J.P.Tite, On the mechanisms of pressure generation in vented explosions, *Combust. Flame* 65 (1986) 1-14.
- [3] V.V. Molkov, A.N. Baratov, A.Y. Korolchenko, Dynamics of gas explosions in vented vessels: a critical review and progress, *Progr. Astronaut. Aeronaut.* 154 (1993) 117-131.
- [4] C.R. Bauwens, J. Chaffee, S.B. Dorofeev, Effect of Ignition Location, Vent Size, and Obstacles on vented Explosion Overpressures in Propane-Air Mixtures. *Combust. Sci. Techol.* 182 (2010) 1915-1932.

- [5] C.R. Bauwens, J. Chaffee, S.B. Dorofeev, Experimental and Numerical Study of Hydrogen-Air Deflagrations in a Vented Enclosure, 7th ISHPMIE Proc. Vol. 1, St. Petersburg, Russia, 2008.
- [6] V.V. Molkov, R. Dobashi, M. Suzuki, T. Hirano, Modelling of Vented Hydrogen-Air Deflagrations and Correlations for Vent Sizing, *J. Loss Prev. Process* 12 (1996) 147-156.
- [7] C.R. Bauwens, J. Chaffee, S.B. Dorofeev, Vented Explosion Overpressures from Combustion of Hydrogen and Hydrocarbon Mixtures, *Int. Journal Hydrogen Energy* 36 (2011) 2329–2336.
- [8] C.R. Bauwens, S.B. Dorofeev, Effect of initial turbulence on vented explosion overpressures from lean hydrogen air deflagrations, *Int. Journal Hydrogen Energy* 39 (2014) 20509-20515.
- [9] R.G. Abdel-Gayed, D. Bradley, M.N. Hamid, M. Lawes, Lewis number effects on turbulent burning velocity, *Proc. Combust. Inst.* 20 (1985) 505-512.
- [10] N. Chakarborty, R.S. Cant, Effects of Lewis number on flame surface density transport in turbulent premixed combustion, *Combust. Flame* 158 (2011) 1768-1787.
- [11] O.K. Sommersel, K. Vaagsaether, D. Bjerketvedt, Hydrogen explosions in 20 ft ISO container, *Int. Journal Hydrogen Energy* 42 (2017) 7740-7748.
- [12] T. Skjold, H. Hisken, S. Lakshmipathy, G. Atanga, M. van Wingerden, K.L. Olsen, M.N. Holme, N.M. Turoy, M. Mykleby, K. van Wingerden, Vented hydrogen deflagrations in containers: Effect of congestion for homogenous mixtures, 2017, <http://doi.org/10.5281/zenodo.998039>.
- [13] L. Wang, R. Quant, A. Kolios, Fluid structure interaction modelling of horizontal-axis wind turbine blades based on CFD and FEA, *J. Wind Eng. Ind. Aerodyn.* 158 (2016) 11-25.
- [14] N. Salaun, A.H. Gronlund, P.E. Nilsen, Risk-based Structural Response against Explosion Blast Loads: Systematic One-to-one CFD (FLACS) / NLFEA (IMPETUS Afea Solver) Coupling to Derive Quantified Response Exceedance, *Chemical Engineering Transactions*, 48, pp. 55-60, 2016.
- [15] M. Malendowski, A. Glema, Development and Implementation of Coupling Method for CFD-FEM Analyses of Steel Structures in Natural Fire, *Procedia Eng.* 172 (2017) 692-700.
- [16] [www.openfoam.org](http://www.openfoam.org).
- [17] A. Yoshizawa, K. Horiuti, A Statistically-Derived Subgrid-Scale Kinetic Energy Model for the Large-Eddy Simulation of Turbulent Flows. *J. Phys. Soc. Japan* 54 (1985) 2834-2839.
- [18] H.G. Weller, G. Tabor, A.D. Gosman, C. Fureby, Application of a flame wrinkling LES combustion model to a turbulent mixing layer, *Proc. Combust. Inst.* 27 (1998) 899-907.
- [19] G. Tabor, H.G. Weller, Large Eddy Simulation of Premixed Turbulent Combustion Using  $\Xi$  Flame Surface Wrinkling Model, *Flow, Turb. Combust.* 72 (2004) 1-27.
- [20] S.P.R. Muppala, N.K. Aluri, F. Dinkelacker, Development of an algebraic reaction rate closure for the numerical calculation of turbulent premixed methane, ethylene, and propane/air flames for pressure up to 1.0 MPa, *Combust. Flame* 140 (2005) 257-266.
- [21] E.M. Burke, A. Singlitico, A. Morones, E.L. Petersen, F. Guthe, BiruteBunkute, R.L. Speth, R.F.D. Monaghan, Progress towards a validated Cantera-based turbulent flame speed solver, *Proc. European Combust. Meeting*, 2015.
- [22] S.P.R. Muppala, M. Nakahara, K.A. Naresh, H. Kido, J.X. Wen, M.V. Papalexandris, Experimental and analytical investigation of the turbulent burning velocity of two-component fuel mixtures of hydrogen methane and propane, *Int. Journal Hydrogen Energy* 34 (2009) 9258-9265.
- [23] J. Goulier, A. Comandini, F. Halter, N. Chayumeix, Experimental study on turbulent expanding flames of lean hydrogen/air mixtures, *Proc. Combust. Inst.* 36 (2017) 2823-2832.
- [24] T. Kitagawa, T. Nakahara, K. Maruyama, K. Kado, A. Hayakawa, S. Kobayashi, Turbulent burning velocity of hydrogen-air premixed propagating flames at elevated pressure, *Int. Journal Hydrogen Energy* 33 (2008) 5842-5849.
- [25] S. A. Verhelst, laminar velocity correlation for hydrogen/air mixtures at spark ignition engine conditions, *Spring Technical Conf. of ASME internal Combust. Engine division, ICE2003*, 2003.
- [26] G. Atanga, S. Lakshmipathy, T. Skjold, H. Hisken, A.G. Hanssen, Structural response for vented hydrogen deflagrations: coupling CFD and FE tools, 2017, <http://doi.org/10.5281/zenodo.1165356>.